Available online at www.sciencedirect.com
ScienceDirect
Journal of Nuclear Materials 363–365 (2007) 915–919
journal of nuclear materials
www.elsevier.com/locate/jnucmat

Simulation of hydrocarbon redeposition in the gaps between divertor tiles

K. Inai [a,*], K. Ohya [b]

[a] Graduate School of Advanced Technology and Science, The University of Tokushima, Minamijosanjima 2-1, Tokushima 770-8506, Japan
[b] Institute of Technology and Science, The University of Tokushima, Tokushima 770-8506, Japan

Abstract

Hydrocarbon redeposition in the gap between divertor tiles is calculated by a Monte Carlo simulation. Using the energy- and species-dependent reflection coefficient on the tile, hydrocarbons repeatedly reflected from the side surfaces redeposit deep in the gap. The calculated results reproduce both the short and long decay lengths of tritium profiles observed on the gap sides of the TFTR bumper limiter [T. Tanabe et al., Fus. Sci. Technol. A 48 (2005) 577]. Redeposition profiles are influenced by the gap width and whether the plasma penetrates the gap or not. At high plasma temperature, the hydrogen concentration of the depositing species in the gap is low due to dissociation of hydrocarbons during long range transport in the plasma. At low plasma temperature, it is high due to deposition of low-energy neutral hydrocarbons, which have a low dissociation probability if the plasma does not penetrate the gap.

PACS: 52.40.Hf; 52.55.Rk; 52.65.Pp

Keywords: Co-deposition; Chemical erosion; Edge modeling; Hydrocarbons

1. Introduction

Recent surface analyses [1,2] have shown that a significant amount of tritium was retained in gap sides between carbon plasma facing components by redeposition of hydrocarbons eroded chemically and transported in edge plasmas. Tritium retention in the tile gaps is a crucial issue because of the difficulty of removal from gaps. Therefore we focus our attention on the influence of plasma condition and redeposition process, e.g. plasma temperature and reflection or sticking coefficient on the top surface of the tile and the gap sides. In this study, the redeposition distribution is calculated and the dominant mechanism for the redeposition in the gap is discussed.

2. Simulation models

Fig. 1 shows a schematic view of the tile and gap configuration used for the calculation. A homogeneous plasma with constant electron and ion temperature, T_e and T_i ($T_e = T_i$), and constant electron density, $n_e = 10^{19}\,m^{-3}$, contacts the top surface of the tile. The angle α of the magnetic field

* Corresponding author. Fax: +81 88 656 7444.
E-mail address: ken-171@ee.tokushima-u.ac.jp (K. Inai).

0022-3115/$ - see front matter © 2007 Elsevier B.V. All rights reserved.
doi:10.1016/j.jnucmat.2007.01.114

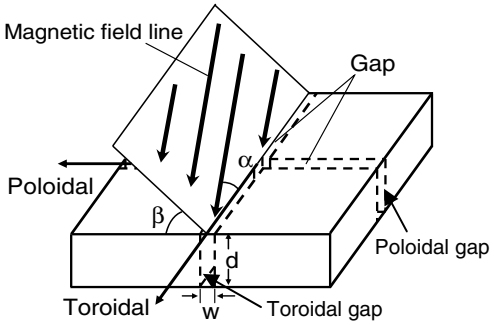

Fig. 1. Schematic view of the assumed tile geometry with toroidal and poloidal gaps ($d = 30$ mm, $w = 3$ mm).

lines with the toroidal direction is 5° and the lines are inclined by $\beta = 30°$ with respect to the poloidal direction; the field strength is 5 T. The rectangular volume above a part of the tile with the surface area of 10×10 cm is the simulation volume, where the thickness of the plasma is 10 cm. A methane molecule (CH_4) is released at a random point of the tile surface with a Maxwellian velocity distribution corresponding to a temperature of 0.1 eV (1160 K). As a result of the collisions with plasma electrons and ions, many neutral and ionized fragments are produced through successive reaction chains. The rate coefficients for possible electron-impact ionization, dissociation, dissociative recombination, proton-impact ionization and charge exchange processes of CH_4 and fragments are calculated using the new complete set of fitting formulae taken from Janev and Reiter [3]. Details of the hydrocarbon transport simulation are given elsewhere [4]. In this study, if a particle produced by a reaction is charged, it is confined by the magnetic field, and experiences the friction and the thermal gradient forces [5] parallel to the magnetic field lines, cross-field diffusion [6], sheath and presheath accelerations [7], and elastic collisions with the residual neutral hydrogen atoms [8]. In the simulation volume, constant electron and ion temperature is assumed. However, the thermal gradient force is important to balance the friction force. Therefore, we assumed the temperature gradient $dT_{e,i}/ds$ is dependent on the plasma temperature linearly, e.g. $dT_{e,i}/ds$ equals 1 eV/m for the plasma temperature 1 eV and $dT_{e,i}/ds$ equals 30 eV/m for the plasma temperature 30 eV, for simplicity. Although the parallel force balance strongly depends on the limiter or divertor characteristics [9]. The ambient hydrogen atom density is taken as 10^{19} m^{-3}. Recently, the reflection (or sticking) coefficients of CH_y ($y \leqq 4$) and C_2H_y ($y \leqq 5$) on a hydrogenated graphite surface for a range of incident energies and angles have been calculated by Alman and Ruzic using molecular dynamics modeling [10]. The energy- and species-dependent reflection coefficients for hydrogenated and amorphized graphite, i.e. 'hard' carbon, are applied for our simulation. According to Alman and Ruzic, the methane family (CH_4, CH_3, CH_2, CH) has rather higher chance of reflection on 'hard' carbon surface, but as the energy is increased, the reflection coefficient of the original hydrocarbon decreases. Furthermore, the dissociation probability at the surface is increased so that the incident hydrocarbon is reflected as part of smaller dissociative fragments. Nevertheless, for C_2H and C_2H_3 Ref. [10] gives reflection coefficients on redeposited hydrocarbon films, i.e. 'soft' surfaces, lower than 70% and 80%, respectively, and in cavity experiments values of reflection coefficient of approximately 10% and 65% were found [11]. When a hydrocarbon is reflected, we assumed that its energy is not changed and the reflection is specular. Since hydrocarbons redeposited on the top surface of the tile are subsequently bombarded with plasma ions, no sticking is assumed, and they are released again in the form of CH_4. On the other hand, around the gaps the distribution of sheath potential (or electric field) is complex, depending on the plasma condition and the gap geometry. Therefore, we assumed the gaps between the tiles are not in direct contact with the plasma, where the sheath acceleration for the ion species does not occur on the gaps, as long as it is not mentioned. Furthermore, if the gaps between the tiles are in direct contact with the plasma, the sheath acceleration occurs toward the gap sides or bottom. Although the whole tiles should have the same value of potential actually. In the simulation, the toroidal and poloidal gaps with width of $w = 3$ mm, and depth of $d = 30$ mm are assumed. CH_4 molecules (10^6) are generated randomly on the top surface.

3. Calculation results and discussion

Fig. 2 shows the number of the redeposited carbon atoms on the side surfaces of both toroidal and poloidal gaps as a function of distance from the rim. Assuming full sticking of hydrocarbons on the side surface ($S_{gap} = 1$), the number of the redeposited carbon atoms decay steeply. Using the energy- and species-dependent reflection coefficient, low-energy hydrocarbons, which are repeatedly

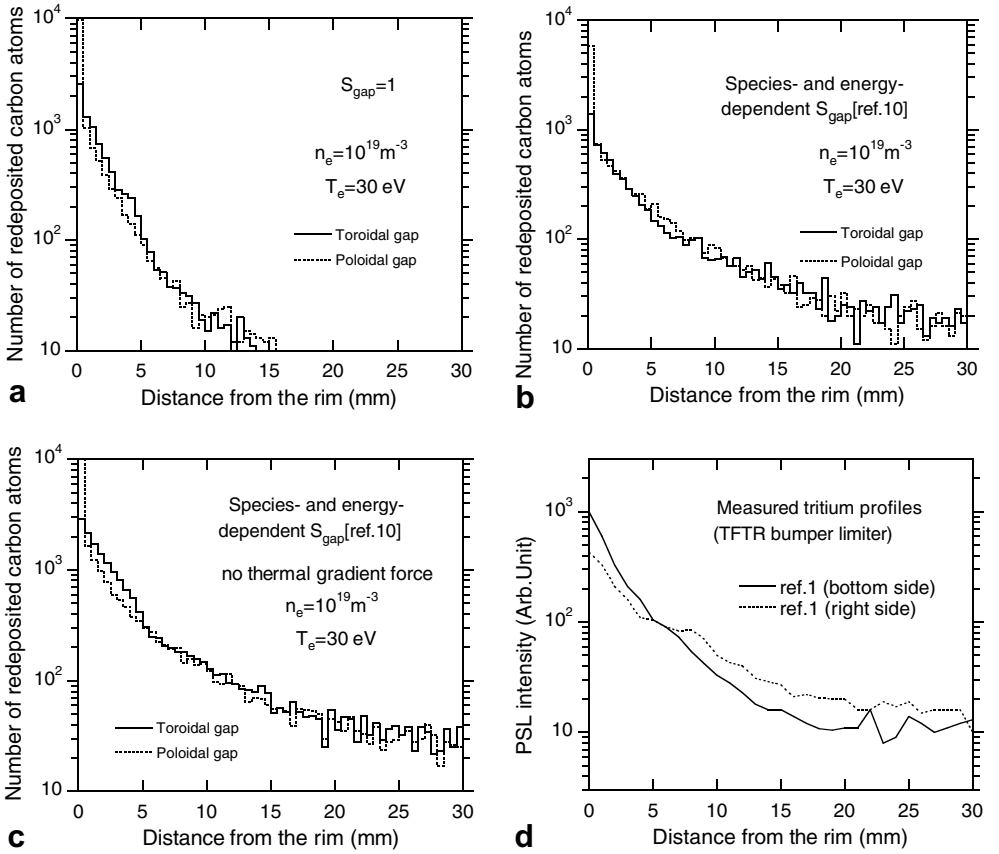

Fig. 2. The number of the redeposited carbon atoms on the side surfaces of both the toroidal and poloidal gaps as a function of distance from the rim for the plasma density of 10^{19} m^{-3} and the plasma temperature of 30 eV. The calculations were done with: (a) sticking coefficient $S_{gap} = 1$, (b) the energy- and species-dependent S_{gap}, (c) the energy- and species-dependent S_{gap} and no thermal gradient force and (d) shows the tritium profiles measured on side surface of the bumper limiter tile from TFTR [1].

reflected from the side surfaces, are able to penetrate deep in the gap, so that the number of the redeposited carbon atoms on the side surface has a longer decay length as shown in Fig. 2(b). The redeposition profile in the toroidal gap with no thermal gradient force on the ion species and using the energy- and species-dependent reflection coefficients (Fig. 2(c)) shows a hump at a distance <5 mm and a gradual decrease at a distance >5 mm, whereas for the profile in the poloidal gap, there is a large peak near the surface and no hump. From analysis of the redeposited species (Fig. 3), the large near-surface peak for the poloidal gap is dominated by highly ionized carbon ions. Carbon ions are redeposited on the side surface of the toroidal gap after a long travel along the magnetic field lines in the gap, producing the hump in the toroidal gap. The parallel force balance strongly depends on the limiter or divertor characteristics. Since the thermal gradient force pushes the ions back into the plasma and thus suppress their redeposition, the hump in the toroidal gap is enhanced without thermal gradient force and, therefore, the difference of the distribution between the toroidal and poloidal gaps is enhanced. The redeposition profiles (Fig. 2(c)) are similar to the tritium profiles of bottom and right side, respectively, of the TFTR bumper limiter tile measured by Tanabe et al. [1] (Fig. 2(d)). There will be a difference between the deposition profiles on the two side surfaces of a gap, due to the magnetic field direction. Nevertheless, two side deposition profiles are summed in these calculations.

Fig. 4(a) and (b) shows the effect of increasing the width of the gap. The distribution of redeposited carbon atoms on the side surface has a longer decay length due to the long range transport of many low-energy ions with larger gyroradii in the gap and also an increased line-of-sight area for neutral hydrocarbons coming from the plasma. Furthermore, in Fig. 4(c), the decay length is influenced by whether

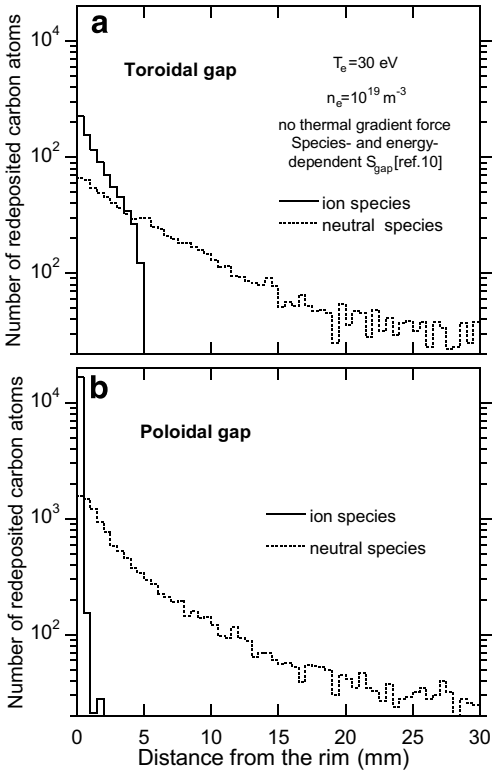

Fig. 3. The number of the redeposited carbon atoms on the side surfaces of both the ion and neutral species as a function of distance from the rim for the plasma density of $10^{19}\,m^{-3}$, the plasma temperature of 30 eV, using the energy- and species-dependent S_{gap} and no thermal gradient force. (a) Toroidal gap, and (b) poloidal gap.

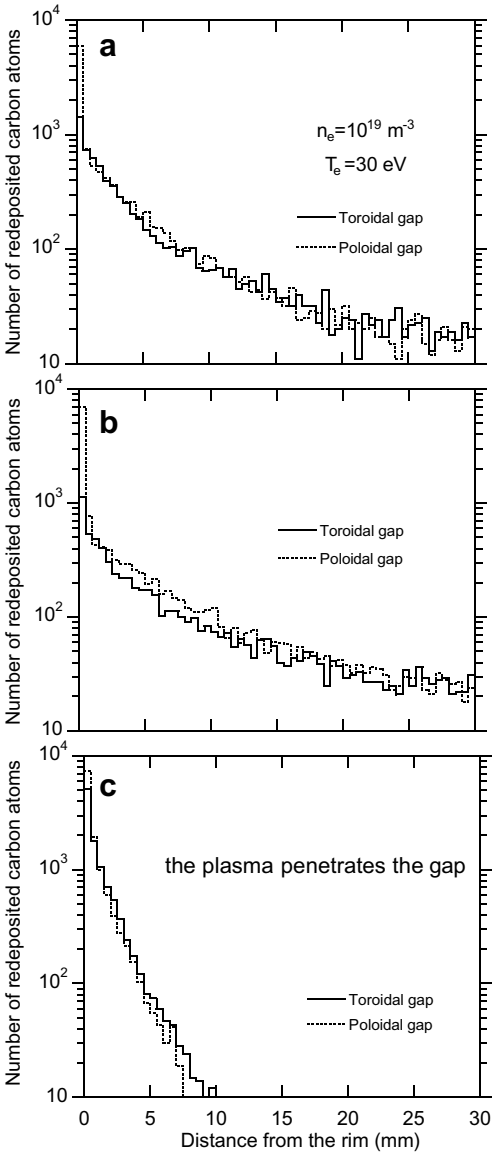

Fig. 4. The number of the redeposited carbon atoms on the side surfaces of the toroidal and the poloidal gaps as a function of distance from the rim for the plasma density of $10^{19}\,m^{-3}$, the plasma temperature 30 eV and the energy- and species-dependent S_{gap}. (a) Gap width = 3 mm, (b) gap width = 5 mm, and (c) gap width = 3 mm and the plasma penetrates the gap.

the plasma penetrates the gap or not. With the plasma filling the gap, the redeposition distribution decay on a short range. This is because ionization and the other mentioned processes take place also inside the gap. At high plasma temperature, many ionized fragments which are accelerated to the side surfaces by the sheath voltage tend to stick the side surface without experiencing any reflection.

The hydrogen concentration of the depositing species, $F_H = H/(C+H)$, is calculated: e.g., $F_H = 0.8$ and $F_H = 0$ for the redeposition in the form of initial CH_4 and fully dissociated carbon, respectively. At high plasma temperature, F_H for the gap sides is low due to dissociation of hydrocarbons during their long range transport in the plasma before redeposition in the gap. When redeposition distribution for the top surface of the tile is calculated in the same condition, F_H is high due to prompt redeposition of CH_4 which is ionized and gyrates back to the surface, as shown in Fig. 5. Using the energy- and species-dependent reflection (or sticking) coefficients, low-energy hydrocarbons are reflected by the top surface of the tile. Furthermore, they are subsequently dissociated in the plasma, and as a result, the F_H is lower than that for full sticking ($S_{surface} = 1$). Hydrocarbons reflected from the side surfaces redeposit on the neighboring side of the gap without transport in the plasma. Therefore, F_H does not change much. Nevertheless, F_H is overly simplified quantity for discussing the realistic hydrogen concentration because

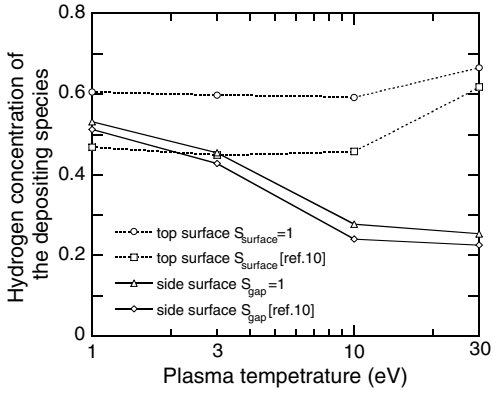

Fig. 5. The hydrogen concentration of the depositing species, $F_H = H/(H + C)$, as a function of plasma temperature at the plasma density of 10^{19} m^{-3} on the top surface of the tile and the side surface in the gap.

of the neglecting processes such as incorporation of H and implantation of H^+, hydrogen depletion due to ion bombardment, and abstraction of surface-bonded hydrogen due to H and hydrocarbon radicals. In addition, the realistic hydrogen concentration stays below a saturation value of roughly 0.4, as found for plasma-deposited a-C:H. Therefore, the realistic hydrogen concentration on the top surfaces will be rather low due to hydrogen depletion as a rather high ion flux. But the redeposits on the gap sides, with a lot of hydrogen, remain in the gap as they are not exposed to the plasma. As a result, at low plasma temperature, the realistic hydrogen concentration is significant in gap sides.

4. Conclusion

Using the energy- and species-dependent reflection coefficient, hydrocarbons are repeatedly reflected from tile side surfaces and they redeposit deep in tile gaps. The calculated results show distributions similar to the observed tritium profiles on a TFTR bumper limiter tile with short and long decay lengths [1]. Redeposition profiles are influenced by the gap width and whether the plasma penetrates the gap or not. At high plasma temperature, the hydrogen concentration of the depositing species, $F_H = H/(H + C)$, in the gaps is low due to dissociation during transport in the plasma. On the tile surface, F_H is high due to the prompt redeposition of CH_4 which is ionized and gyrates back to the surface. However, the realistic hydrogen concentration will be rather low due to hydrogen depletion as a rather high ion flux. At low plasma temperature, F_H in the gap is higher due to deposition of low-energy neutral hydrocarbons with low dissociation probability if the plasma does not penetrate the gap.

References

[1] T. Tanabe et al., Fus. Sci. Technol. 48 (2005) 577.
[2] W.L. Hsu et al., J. Vac. Sci. Technol. A 7 (1989) 1065.
[3] R.K. Janev, D. Reiter, Rep. Forschungszentrum Jülich, Jül-3966, 2002.
[4] K. Ohya, T. Tanabe, J. Kawata, Fus. Eng. Des. 81 (2006) 205.
[5] P.C. Stangeby, The Plasma Boundary of Magnetic Fusion Devices, IOP, Bristol, 2000, p. 296.
[6] K. Shimizu, H. Kubo, T. Takizuka, et al., J. Nucl. Mater. 220–222 (1995) 410.
[7] J.N. Brooks, Phys. Fluids B 2 (1990) 1858.
[8] T. Motohiro, Y. Taga, Thin Solid Films 112 (1984) 161.
[9] K. Shimizu, T. Takizuka, A. Sakasai, J. Nucl. Mater. 241–243 (1997) 167.
[10] D.A. Alman, D.N. Ruzic, Phys. Scr. T 111 (2004) 145.
[11] C. Hopf et al., J. Appl. Phys. 87 (2000) 2719.